

lifetime and the relaxation process to the ground state are not known, and either may account for the enhanced reactivity at untilted dimer sites.

The ability to prepare dimers on a Si(100) surface has implications beyond the present system. There are many surface reactions that yield a range of unexpected products. The product distribution may reflect the dynamics of the surface atoms involved, and the detailed mechanisms of such reactions may be studied by the present method. Although untilted dimer sites can be generated by adsorption of other species such as halogens, the use of hydrogen is particularly attractive. Hydrogen is both small and electroneutral, so that other than pinning the geometry at adjacent dimer sites, it does not unduly influence the chemistry that takes place at these sites. This method is also likely to be important for other semiconductor systems because the charge density on these surfaces will generally be insufficient to screen chemically induced lattice distortions from neighboring sites.

References and Notes

1. D. J. Doren, *Adv. Chem. Phys.* **95**, 1 (1996).
2. M. L. Wise, B. G. Koehler, P. Gupta, P. A. Coon, S. M. George, *Surf. Sci.* **258**, 166 (1991).
3. Z. Jing, J. L. Whitten, *J. Chem. Phys.* **98**, 7466 (1993).
4. K. W. Kolasinski, W. Nessler, A. Meijere, E. Hasselbrink, *Phys. Rev. Lett.* **72**, 1356 (1994).
5. K. W. Kolasinski, W. Nessler, K. Bornscheuer, E. Hasselbrink, *J. Chem. Phys.* **101**, 7082 (1994).
6. P. Bratu, K. L. Kompa, U. Hofer, *Chem. Phys. Lett.* **251**, 1 (1996).
7. P. Bratu *et al.*, *Phys. Rev. B* **54**, 5978 (1996).
8. K. W. Kolasinski, S. F. Shane, R. N. Zare, *J. Chem. Phys.* **96**, 3995 (1992).
9. E. Pehlke, M. Scheffler, *Phys. Rev. Lett.* **74**, 952 (1995).
10. P. Kratzer, B. Hammer, J. K. Nørskov, *Chem. Phys. Lett.* **229**, 645 (1994).
11. W. Brenig, A. Gross, R. Russ, *Z. Phys. B* **96**, 231 (1994).
12. P. C. Weakliem, G. W. Smith, E. A. Carter, *Surf. Sci. Lett.* **232**, L219 (1990).
13. M. R. Radeke, E. A. Carter, *Phys. Rev. B* **54**, 11803 (1996).
14. E. M. Lauridsen *et al.*, *Surf. Sci.* **453**, 18 (2000).
15. Experiments were carried out in an Omicron Variable Temperature STM (VT-STM) system that has a base pressure of $\sim 5 \times 10^{-11}$ torr. The STM was operated in constant current mode with the tunneling bias applied to the tip. Images were recorded at +2 V and -2 V, voltages low enough to ensure that the tip did not induce hydrogen desorption (23). Sample cooling was accomplished by pumping liquid N₂ or He through a continuous flow cryostat that was thermally coupled to the sample via a copper braid and clamping mechanism. Clean Si(100)-2 \times 1 surfaces were prepared by heating the Si(100) substrate (1ohm-cm, phosphorus doped) to ~ 1350 K to desorb the native oxide and were then cooled slowly to form a good 2 \times 1 reconstruction. Hydrogen-passivated Si(100)-2 \times 1 surfaces were prepared by dosing the clean surface with atomic hydrogen while the substrate temperature was held at ~ 600 K. Molecular adsorption experiments were performed using both hydrogen and deuterium, with similar results. The dosing gas was cooled by liquid N₂ before dosing to remove all traces of reactive contaminants (primarily H₂O). Dosing was performed by back-filling the preparation chamber with room-temperature H₂ or D₂ to a pressure of 5.0×10^{-7} torr. All ion pumps and filaments were turned off, and the exposures described were corrected for the detection efficiency of H₂.
16. R. A. Wolkow, *Phys. Rev. Lett.* **68**, 2636 (1992).

17. J. J. Boland, *Phys. Rev. Lett.* **67**, 1539 (1991).
18. J. E. Northrup, *Phys. Rev. B* **47**, 10032 (1993). This paper describes an energy gap of about 1 eV, but the method used underestimates the true gap by at least 0.5 eV.
19. P. Kratzer, E. Pehlke, M. Scheffler, M. B. Raschke, U. Hofer, *Phys. Rev. Lett.* **81**, 5596 (1998).
20. A. Biedermann, E. Knoesel, Z. Hu, T. F. Heinz, *Phys. Rev. Lett.* **83**, 1810 (1999).
21. F. M. Zimmermann, X. Pan, *Phys. Rev. Lett.* **85**, 618 (2000).
22. If ψ_L and ψ_R are the wave functions corresponding to the Si-H bonds on the left and right side of the H-filled dimer then the wave function for the entire dimer can

be written as $(\psi_L + \psi_R)^2 (\psi_L - \psi_R)^2$, which is odd with respect to reflection across the dimer bond. Because the interaction in the H₂ product is bonding (i.e., even), if symmetry is conserved then the bare dimer produced immediately after desorption must have odd symmetry, representing an excited state of the dimer.

23. T. C. Shen, P. Avouris, *Surf. Sci.* **390**, 35 (1997).
24. We thank W. A. Goddard III and J. E. Northrup for valuable discussions. Financial support for this work was provided by the National Science Foundation under Contract DMR 9812416, and is gratefully acknowledged.

5 July 2000; accepted 21 August 2000

Detection of Daily Clouds on Titan

Caitlin A. Griffith,¹ Joseph L. Hall,¹ Thomas R. Geballe²

We have discovered frequent variations in the near-infrared spectrum of Titan, Saturn's largest moon, which are indicative of the daily presence of sparse clouds covering less than 1% of the area of the satellite. The thermodynamics of Titan's atmosphere and the clouds' altitudes suggest that convection governs their evolutions. Their short lives point to the presence of rain. We propose that Titan's atmosphere resembles Earth's, with clouds, rain, and an active weather cycle, driven by latent heat release from the primary condensable species.

Titan possesses an atmosphere often compared to that of Earth. It is composed mainly of N₂, with a surface pressure of 1.5 bar (150 kPa), and possesses a wealth of organic material. Moreover, Titan may support a methane cycle, resembling Earth's hydrologic cycle, with clouds, rain, and seas (1, 2). In the past decade, dozens of images and spectra have been recorded through narrow spectral regions or "windows," where Titan's otherwise optically thick atmosphere is largely transparent. However, no indication was found for the presence of rain and oceans, which are difficult to ascertain by remote measurements. Observations also showed no evidence (3-9) of clouds (relatively easy to detect), with one exception (10).

On 4 and 5 September 1995, spectra recorded within four windows revealed flux enhancements of 14 to 200%, indicative of the presence of a hurricane-sized cloud system (10). This first appearance of clouds challenged our understanding of weather on a planetary body similar to, yet intriguingly different from Earth, while providing insufficient data (one event) for its investigation. Compared to Earth, Titan's atmosphere is cooler, more massive, and thus essentially more sluggish. Titan spins slowly, providing little vorticity to cloud systems. In addition, Titan receives ~ 100 times less power from the sun (Table 1).

To investigate Titan's weather, we recorded repeated observations within three spectral

windows. We obtained 21 spectra at 1.8- to 2.4- μ m wavelength, 10 spectra at 1.5 to 1.8 μ m, and 15 spectra at 2.4 to 3.0 μ m in September 1999. These data are supplemented by five spectra from 1993 and 1997 (Table 2). Titan's 1.8- to 2.4- μ m albedo (Fig. 1) manifests characteristics of the moon's surface, stratosphere, and troposphere. Prominent flux variations occurred at 2.0 to 2.11 μ m, where Titan's atmosphere is most transparent, and result from Titan's surface as different terrains rotate into view (Fig. 1). No variations appeared at 2.17 to 2.4 μ m, where sunlight reflects from Titan's stratosphere, which does not observably change over a fortnight. Subtle variations emerged at 2.12 to 2.17 μ m, where sunlight penetrates deep into Titan's atmosphere but does not reach the surface. These indicate the presence of variable cloud coverages (11).

To better discern the spectral variations, we calculated the difference between each spectrum and that with the lowest 2.11- to 2.17- μ m albedo (the second observation of 14 September 1999, spectrum 6b in Table 2). The 2.11- to 2.17- μ m flux variations emerge clearly in contrast to the noise at 2.17 to 2.4 μ m and the uncorrelated surface variations shortward of 2.11 μ m (Fig. 2). Most notably, these flux enhancements consistently occur at ~ 2.155 μ m (Fig. 2). In addition, variations arise in spectra recorded 2 hours apart (Table 2) [Web fig. 1 (12)].

The 1.5- to 1.8- μ m observations indicate variations consistent with those recorded at 2.11 to 2.17 μ m (Fig. 2). Among the noisy 2.4- to 3.0- μ m data, only the 22 September

¹Department of Physics and Astronomy, Northern Arizona University, Flagstaff, AZ 86011-6010, USA.
²Gemini Observatory, Hilo, HI 96720, USA.

REPORTS

1999 spectrum revealed a flux enhancement above the $1\text{-}\sigma$ noise level of 0.0008. This $2.9\text{-}\mu\text{m}$ flux exceeded by 0.0004 to 0.002 that observed on 14 September 1999 at 13:57 UT (universal time), in agreement with the high fluxes measured on 22 September 1999 at 1.62 and $2.14\ \mu\text{m}$.

To investigate the cause for the observed flux variations, we analyzed the spectra with radiative transfer calculations. Titan's surface

albedo and haze opacity are derived from the 2.0- to $2.11\text{-}\mu\text{m}$ and 2.18- to $2.3\text{-}\mu\text{m}$ spectra, respectively (11). The abundances of methane or other gases in Titan's atmosphere do not highly affect Titan's 2.11- to $2.17\text{-}\mu\text{m}$ albedo (11). Thus, the one remaining variable, the cloud coverages (13), is independently determined from the 2.11- to $2.17\text{-}\mu\text{m}$ spectra (14). We find that the addition of highly reflective particulates, characteristic

of methane clouds, uniquely reproduces the degree of enhancement and the spectral morphology of the observed variations (Fig. 3).

Uncertainties in the methane line parameters lead to small discrepancies (e.g., at $1.63\ \mu\text{m}$) between the observed and synthetic spectra (Fig. 3). To evaluate the spectral variations fairly independently of these uncertainties, we modeled the residuals. We calculated two spectra, one of a cloudy day and the other of a clear day (i.e., spectrum 6b). The differences between the spectra are compared to the differences between the observations. These calculations determine the extents and altitudes of Titan's clouds (11). The wavelength where the flux enhancement begins establishes the cloud tops (Fig. 3). The degree of enhancement provides the coverage of Titan's clouds (assumed optically thick) (15).

Analysis of the spectra reveals that clouds reside at the same altitude of $\sim 27\ \text{km}$, cover $\sim 0.5\%$ of Titan's disk, and can dissipate in 2 hours. In contrast, Titan's large cloud system of 5 September 1995 lived for ≥ 2 days, displayed cloud tops at $\sim 16\ \text{km}$, and covered 5 to 7% of the moon's disk. Because the large cloud system was witnessed only once, its nature and its relationship to the frequent clouds is obscure. In contrast, traits of the smaller daily clouds divulge the processes involved in their evolutions.

The common heights of Titan's daily clouds suggest that a common process governs their development. One mechanism is convection. Although Titan's troposphere is deficient in the high thermal gradients that trigger much of Earth's weather (16) and in the solar energy that fuels it, Titan has more latent heat (per unit surface area) than does Earth. Assuming saturated conditions, 33 times more methane exists per volume of Titan's atmosphere at the surface than water in Earth's atmosphere (Table 1). The latent heat available renders air parcels more buoyant upon condensation. Resulting convectively evolved clouds display heights governed primarily by Titan's thermal profile, methane abundance, and the degree of mixing experienced by the rising air with the environment. Because Titan's thermal profile and humidity are probably fairly uniform, convection should produce clouds of fairly uniform heights. Titan's thermal profile further suggests convection, because below $\sim 15\ \text{km}$, the profile is conditionally unstable, i.e., the atmosphere is unstable to convection if saturated (17–19). Such a profile, typical in convective regions of Earth's tropics, reflects the average of dry regions of subsistence and wet regions of convection (20).

From Titan's thermal profile and its range of possible methane humidities, we estimate the altitude of convective clouds. The stability of Titan's atmosphere can be understood by considering Titan's equivalent potential

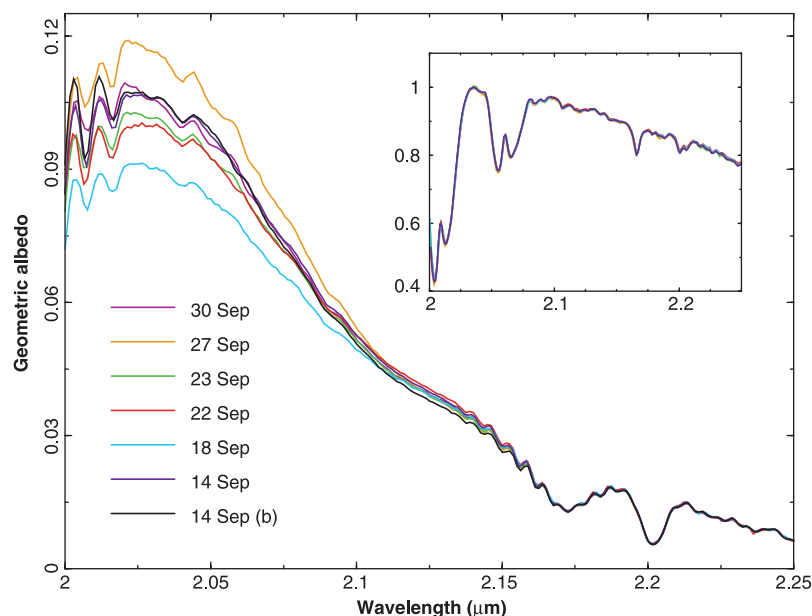


Fig. 1. Observations of Titan and the calibration G0 IV star (inset) recorded at the United Kingdom Infrared Telescope (Mauna Kea, Hawaii), equipped with its CGS4 spectrometer. Shown are the first spectrum recorded each night, along with the second recorded on 14 September 1999 [14 Sep (b)]. The seven spectra of the standard star (BS635) (inset) confirm sound operation of the spectrometer and indicate no systematic effect that would produce the flux variations in Titan's 2.12- to $2.17\text{-}\mu\text{m}$ spectra. Division of Titan's raw spectrum by that of the G star eliminates telluric absorption features. Multiplication by geometric factors that account for Titan's size and distance from Earth and the sun provides Titan's geometrical albedo (the reflection from Titan relative to a Lambert surface, i.e., a diffuse perfect radiator). To allow comparison between observations (given photometric uncertainties), Titan's spectra are normalized to match at $2.20\ \mu\text{m}$, which samples Titan's stratosphere. Globally averaged, the moon's stratosphere does not measurably vary over a 2-week period. Errors in the absolute albedo of 10% do not significantly affect the analysis of spectral variations and the determination of cloud characteristics (3). The 3σ error in Titan's albedo is ≤ 0.0002 at 2.0 to $2.3\ \mu\text{m}$.

Table 1. A comparison between various physical and atmospheric characteristics for Titan and Earth. Km am, kilometer amat (1 km am = 2.69×10^{24} molecules/cm²).

Parameter	Earth	Titan
Main constituent	N ₂	N ₂
Surface pressure	1 bar	1.5 bar
Major condensible	Water	Methane
Surface temperature	288 K	94 K
Solar flux (W/m ²)	1368	15
Gravity (m/s ²)	9.82	1.35
Vertical column density	8 km am	91 km am
Seed nuclei (cm ⁻³)	$\sim 10^3$ to 10^5	~ 10 to 50
Typical cloud coverage	50%	$\leq 1\%$
Heat of vaporization (J/mol)	4.1×10^4	8.2×10^3
Surface number density (cm ⁻³)	2.6×10^{19}	1.2×10^{20}
Saturated mixing ratio	0.017	0.12
Period of rotation	1 day	15.95 days
Radiative time constant	~ 4 months	~ 130 years*

*Value for Titan is taken from Gierasch *et al.* (32).

REPORTS

temperature, θ_e , and the equivalent potential temperature, θ_e^* , of a saturated atmosphere having Titan's thermal profile (20). These quantities are defined in terms of the potential temperature, θ , the temperature an air parcel (of pressure P and temperature T) would have if it expanded adiabatically to a standard pressure, P_s (taken here as the surface pressure). Thus, $\theta = T \left(\frac{P_s}{P} \right)^{R/c_p}$, where R is the gas constant and c_p the specific heat at constant pressure. This is conserved for dry adiabatic motion. A similar quantity, conserved for wet adiabatic motion is θ_e , the potential temperature that a parcel would have if all the methane were condensed, allowing the latent heat to warm the parcel. Its value can be approximated by $\theta_e \sim \theta \exp(L_c q_s / c_p T)$, where L_c is latent heat of condensation and q_s is the saturation mixing ratio.

The stability of an atmosphere with respect to displacements in a saturated atmosphere can be expressed in terms of $\frac{\partial \theta_e^*}{\partial z}$, a measure of the relative temperature change and therefore density change between a saturated environment and pseudoadiabatically displaced parcel. A negative slope indicates conditional instability, a positive slope stability. A plot of Titan's thermal profile in terms of θ_e^* portrays the well-known stability of Titan's atmosphere (Fig. 4). Titan's atmosphere is unstable to the displacements of saturated air below ~ 15 -km altitude and stable above 15 km.

Voyager measurements of Titan's thermal profile imply sub-saturated surface conditions of $\leq 60\%$ humidity at the two positions sampled (19, 21). Under these conditions, a parcel of surface air will not convect readily; instead it must be raised until saturated at the lifting condensation level (LCL) and further lifted until sufficient latent heat renders the parcel buoyant at the level of free convection (LFC). The altitude to which air, if lifted, will convect freely (the LFC) can be determined by plotting the θ_e for an assumed vertical profile of the methane abundance. Adiabatically lifted air conserves θ_e , becoming buoyant when the parcel's θ_e exceeds θ_e^* . The LFC altitude, dependent on the methane mixing ratio of the parcel, is 5.5 km for a surface parcel of 60% humidity (Fig. 4). A parcel more humid than that measured by Voyager will have a lower LFC, e.g., 2 km for a parcel of 80% humidity (22). The range of methane abundances on Titan is presently unknown. Yet, under subsaturated surface conditions, the formation of cumulus clouds on Titan requires a process that raises air to its LFC (23). Similarly, dynamical lifting is required on Earth where a typical tropical thermal profile indicates a LFC at 1.5 km.

A rising parcel remains buoyant until it reaches the level where its θ_e is smaller than

θ_e^* , and overshoots this altitude by several kilometers as a result of the momentum gained on ascent. Yet, buoyant parcels sometimes do not conserve θ_e because drier environmental air is entrained in the parcel, making it less buoyant (24). If we consider entrainment rates typical of Earth's cumuli and

a range of possible methane profiles, we find that parcels of 25%, 60%, and 80% humidity remain buoyant up to 20- to 23-km, 8- to 25-km, and 15- to 28-km altitude, respectively (Fig. 4). Thus, in agreement with studies of the dynamics of Titan's atmosphere (23), we find that convective clouds do not form be-

Fig. 2. Residuals of Titan's spectra indicate activity in Titan's troposphere, probed at 2.11 to 2.17 μm and 1.62 to 1.63 μm . (Left) The difference between the first spectrum recorded each evening and the second spectrum recorded on 14 September 1999 (6b, Table 2). (Right) The difference between the first 1.62- μm spectrum recorded each evening (at 11:45 UT on 18 September 1999, 11:27 UT on 22 September 1999, 11:13 UT on 23 September 1999, 11:02 UT on 27 September 1999, and 11:42 UT on 30 September 1999) and the spectrum recorded on 14 September 1999 (at 13:07 UT). The 1.62- μm changes are small compared to the 2.11- to 2.17- μm modulations, because the higher optical depth of overlying haze at 1.62 μm mutes the effects of clouds below. In addition, although the errors due to noise equal those at 2.14 μm , a systematic error of 0.0005 arises as a result of the steep spectral slope sampled at 1.62 μm and its sensitivity to the wavelength calibration. Nonetheless, the 1.62 μm variations correlate with those observed at 2.14 μm . The flux was highest early in the evening of 22 September, lowest late on 14 September, and intermediate on the other 4 days.

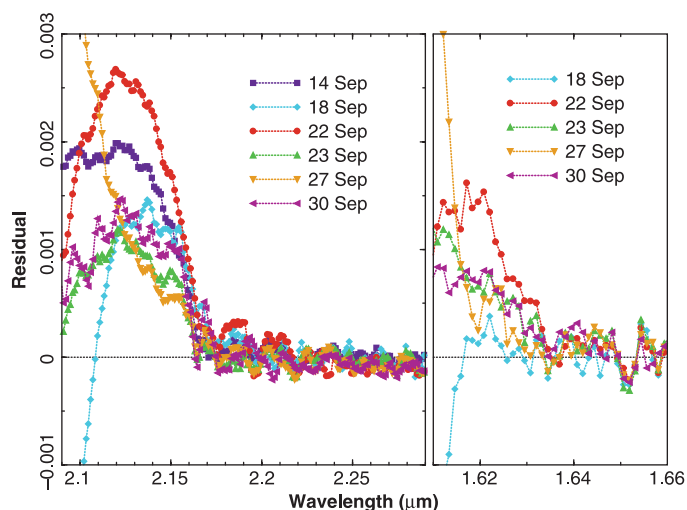


Fig. 3. (A) Radiative transfer calculations of Titan's spectra. Observations (black diamonds) 6a and 7a (Table 2) are shown with 7a offset by 0.01 for greater clarity. In the spectral region displayed, Titan's surface is not observed. Also shown are calculations that assume optically thick clouds at 24 to 30 km (red lines), with coverages of 0.45 and 0.37% for the 14 and 18 September data, respectively. The cloudless models (blue lines), in comparison, show that clouds reflect sunlight and thus elevate Titan's 2.11- to 2.17- μm flux to the observed level. (B and C) Models of the differences between Titan's spectra provide a measure of the altitudes of Titan's clouds. Spectra are fit with clouds at different altitudes. These are subtracted by cloudless spectra. (B) The 1999 data. Observation 6b is subtracted from 6a, and the difference is depicted by black squares. Cloud coverages were ascertained by fitting Titan's 2.13- μm albedo. Coverages of 0.93, 0.68, 0.53, 0.45, and 0.4% were derived for clouds at 12-, 16-, 21-, 27-, and 35-km altitude, respectively. Clouds at 27 km best match the observed spectra. (C) The 1995 data. Titan's spectrum recorded on 5 September 1995 is subtracted by observation 1 (black squares). Coverages of 6, 5, 3.5, 3, and 2.6% were derived for clouds at 12-, 16-, 21-, 27-, and 35-km altitude, respectively. Clouds at 16 km best match the observed spectra. The uncertainty in the methane distribution, assuming half to two times the nominal distribution, provides an uncertainty of 5 km in the altitude of the clouds.

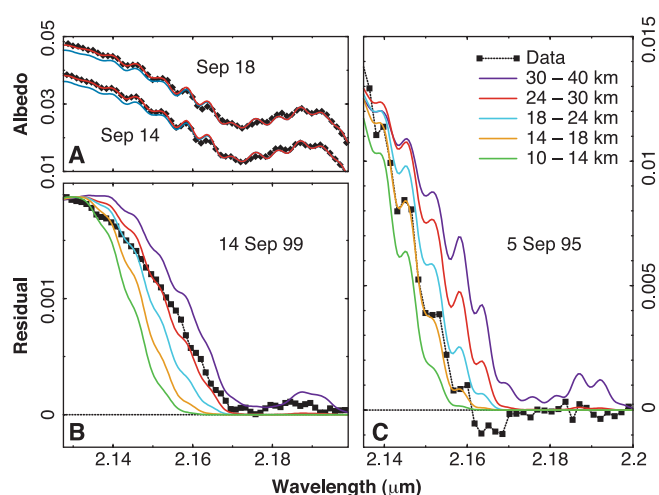


Fig. 4. The stability of Titan's atmosphere to convection is shown with calculations of Titan's effective temperature (dot-dashed line), its θ_e^* profile (solid line), and the θ_e profile, assuming a 60% subsaturated troposphere (thick gray line). Adiabatically lifted air, starting with 60% humidity at the ground, saturates 2 km above the surface (LCL) and becomes buoyant 5.5 km above the surface (LFC). A parcel rising without mixing with the ambient air preserves its θ_e (dashed line). A rising parcel that mixes with the environment does not conserve θ_e (dotted line). Here, the parcel's humidity was taken to be 60% at the surface, and the environmental air was assumed to be 60% subsaturated throughout the troposphere. The entrainment rate is parametrized by a plume of radius 4 km (24). The level at which the parcel's θ_e is smaller than θ_e^* marks the point at which the parcel is no longer buoyant. The air will nevertheless rise a little further as a result of its momentum. Calculations assume the thermal profile of (21); the thermal profiles of (19) provide similar results.

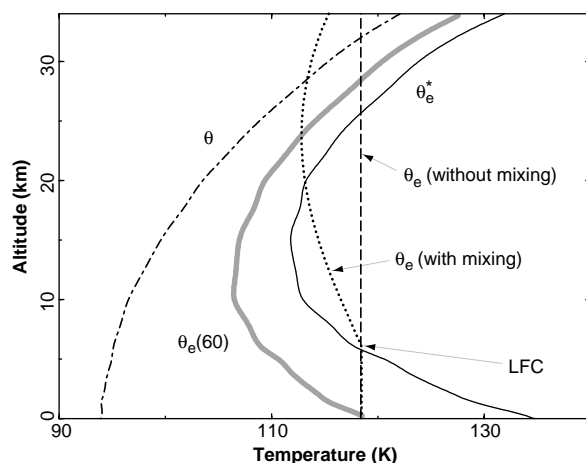


Table 2. Log of 1.8- to 2.4- μm spectra and derived cloud coverages. The spectral type of the calibration star, BS635, is G0 IV. All observations, taken with CGS4's 40 1/mm grating, have a resolving power of 400.

Spectrum number	Date (UT)	Time (UT)	Central longitude*	Air mass†	Coverage (%)
1	13 Sep 1993	09:00	53	1.27 ⁰	0.0
2	30 Sep 1993	06:00	75	1.37 ⁶	0.2
3	27 Jul 1997	15:22	230	1.03 ¹³	0.6
4	17 Oct 1997	07:47	278	1.18 ⁵	0.0
5	26 Oct 1997	08:30	123	1.05 ⁸	0.3
6 a,b	14 Sep 1999	11:37/13:44	149	1.18 ⁷ /1.01 ²	0.5/0.0
7 a,b,c	18 Sep 1999	11:31/12:48/15:04	240	1.18 ¹ /1.03 ¹ /1.08 ²	0.4/0.4/0.4
8 a,b,c	22 Sep 1999	11:15/12:33/15:01	330	1.15 ⁹ /1.03 ¹ /1.11 ²	0.7/0.3/0.3
9 a,b,c	23 Sep 1999	11:03/12:14/14:23	352	1.18 ⁴ /1.03 ¹ /1.05 ³	0.2/0.3/0.3
10 a,b,c	27 Sep 1999	10:50/12:02/14:24	83	1.17 ¹ /1.04 ² /1.08 ¹	0.2/0.2/0.2
11 a,b,c	30 Sep 1999	11:29/12:08/12:59	150	1.06 ² /1.02 ⁰ /1.01 ⁰	0.4/0.4/0.2
12 a,b,c	30 Sep 1999	13:08/13:25/13:35	152	1.01 ⁰ /1.02 ⁰ /1.03 ⁰	0.2/0.2/0.2

*Titan's leading and trailing hemispheres are observed at longitudes 87° and 269°, respectively. †The superscript values are the differences between the air masses of Titan and the standard star, in hundredths of air mass.

low 7 km. In addition, the abundant latent heat on Titan causes humid air, if raised to its LFC, to advance to altitudes of ~25 km, where clouds are observed.

The lifetimes of Titan's clouds further elucidate their evolution. On 14 and 22 September, clouds dissipated in a couple of hours (Table 2). Such rapid evolution suggests the presence of rain. Sedimentation rates, as a function of particle size, indicate that particles must accumulate into mm-sized raindrops (25) to fall tens of km (out of sight) in 2 hours.

Titan's weather, while perhaps endowed with terrestrial character such as rain and convective plumes, betrays an exotic disposition: a sparse cloudiness interrupted rarely by cloud systems 20 times larger than those normally observed. Titan's cloud coverages (~0.5%) compare meagerly with terrestrial values (35 to 70%). Also unlike Earth, Titan's daily clouds reach a common height. These characteristics suggest that latent heat

plays a larger role in fueling Titan's weather than it does on Earth, where solar irradiation dominates. Observations do not yet reveal processes that initiate cloud formation, which are often unrelated to those that sustain and evolve clouds. The local terrain, topography, winds, and humidity on Titan are unknown. In addition, data do not sample enough of Titan's disk to ascertain whether clouds prefer particular regions of Titan's globe (Table 2), and are thus incited by surface features. The mysterious instigator of activity in this cool and slothful atmosphere will be examined with future ground-based observations and by the Cassini spacecraft encounter with Titan in 2004.

References and Notes

1. F. M. Flasar, *Science* **221**, 55 (1983).
2. J. I. Lunine, D. J. Stevenson, Y. L. Yung, *Science* **222**, 1229 (1983).
3. C. A. Griffith, T. Owen, R. Wagener, *Icarus* **93**, 362 (1991).

4. M. T. Lemmon, E. Karkoschka, M. Tomasko, *Icarus* **103**, 329 (1993).
5. C. A. Griffith, *Nature* **364**, 511 (1993).
6. A. Coustenis, E. Lellouch, J. P. Maillard, C. P. McKay, *Icarus* **118**, 87 (1995).
7. M. T. Lemmon, E. Karkoschka, M. Tomasko, *Icarus* **113**, 27 (1995).
8. P. H. Smith *et al.*, *Icarus* **119**, 336 (1996).
9. M. Combes *et al.*, *Icarus* **129**, 482 (1997).
10. C. A. Griffith, T. Owen, G. A. Miller, T. Geballe, *Nature* **395**, 575 (1998).
11. The variable methane absorption in Titan's spectrum allows us to vertically resolve Titan's atmosphere. In the deep methane bands (e.g., 2.17 to 2.4 μm), sunlight penetrates to altitudes only above 50 to 80 km altitude before being fully attenuated. The non-zero albedo provides a measure of the optical depth and effective particle size of Titan's haze in the lower stratosphere (10). We used the haze profile derived by (3, 10). At progressively weaker methane absorption, lower altitudes are reached. Titan's 5 to 30 km altitude (where methane can condense) is investigated using Titan's 2.12- to 2.17- μm spectrum. The surface is established from the moon's 2.0- to 2.11- μm albedo. We used doubling and adding techniques (26) to approximate the equation of radiative transfer, along with line-by-line and Mie scattering calculations to incorporate gas absorption and the scattering by particulates (3, 10). Our nominal methane distribution is that of (3): a 60% humidity at Titan's surface, above which the mixing ratio is fixed until saturation is reached, and a saturated mixing ratio above this point up to the tropopause, above which the mixing ratio is held constant at the tropopause value. We note that changes in the methane abundance (as high as a halving or doubling of this distribution) fail to reproduce the observed flux variations.
12. Supplementary fig. 1 is available at www.sciencemag.org/feature/data/1054124.shl
13. On the basis of the rapid variations in Titan's spectra, we assume the cause is a local one, i.e. that the implied clouds that we see varying are discrete local events rather than a global and thin veil of clouds across Titan's disk that changes everywhere simultaneously.
14. The 1.62- μm spectra (Fig. 2) are not fully analyzed with radiative transfer calculations, because there are no measurements of the line parameters and energy levels that characterize the methane absorption in this spectral region. If we assume, however, that the opacity at 1.62 μm equals that at 2.14 μm , we find that the enhancement of Titan's 1.62- μm flux is approximately half that at 2.14 μm , as a result of the clouds. This estimate matches the spectral behavior we observed (Fig. 2). Analysis of the 2.95- μm spectrum also suffers from uncertainties in the methane absorption parameters. If we adopt the values derived in (10), we find that the 2.95- μm flux enhancement is about ~85% of that at 2.14 μm . This is consistent with the enhancement observed on 22 September 1999.
15. Uncertainties in the methane abundance and line parameters generate uncertainties in the coverage and the heights derived for the clouds. We find that the methane absorption reproduces the transmittance of Titan's atmosphere reliably for wavelengths between 2.125 and 2.4 μm . Between 2.12 and 2.125 μm , the methane absorption coefficients used (3) provide too little absorption, rendering the atmosphere more sensitive to the surface than the data indicates. We therefore consider only the 2.125- to 2.17- μm spectral region to derive cloud properties. This has led us to revise the original estimate by Griffith *et al.* (10) regarding the coverage of the clouds on 4 and 5 September 1995; we now derive a 5 to 7% coverage, not the 9% coverage of the original paper.
16. F. M. Flasar, R. E. Samuelson, B. J. Conrath, *Science* **292**, 693 (1981).
17. V. R. Eshleman, G. F. Lindal, G. L. Tyler, *Science* **221**, 53 (1983).
18. D. M. Hunten *et al.*, in *Saturn*, T. Gehrels, M. S. Matthews, Eds. (Univ. of Arizona Press, Tucson, AZ, 1984), pp. 671-759.

19. C. P. McKay, S. C. Martin, C. A. Griffith, R. M. Keller *Icarus* **129**, 498 (1997).
 20. J. R. Holton, *An Introduction to Dynamical Meteorology* (Academic Press, San Diego, CA, 1992).
 21. E. Lellouch *et al.*, *Icarus* **79**, 328 (1989).
 22. The LFC for supersaturated conditions in the mid to upper troposphere, as suggested by Courtin *et al.* (27) and Samuelson *et al.* (28), significantly exceeds those for saturated conditions. At 140% ambient supersaturation, the LFC lies at 13 km altitude for a parcel of 60% humidity starting at the surface.
 23. M. Awai, J. L. Lunine, *Geophys. Res. Lett.* **21**, 2491 (1994).
 24. The entrainment of local air breaks the conservation of θ_e for the rising plume. The increasing mass of a plume parcel, m , is parametrized as $\frac{1}{m} \frac{dm}{dz} = \frac{\alpha}{r}$

following laboratory simulations (29) in studies of clouds in Earth's tropics (30). Observations of terrestrial clouds indicate a value of $\alpha = 0.2$ and range of plume radii of $r = 0.6$ to 4 km.
 25. The presence of rain agrees with the paucity of nucleation sites available in Titan's atmosphere (Table 1). In the terrestrial atmosphere, the initial size of a raindrop is roughly determined by the number of drops and the mass needed to lower a supersaturated atmosphere back to saturation. The existence of only a few nucleation sites brings about few cloud particles and large particle sizes. The only known source of nucleation sites on Titan is its haze, the number density of which is several orders of magnitude smaller than typical terrestrial values. Considering the low number density of nucleation sites compared to the high methane abundance, Toon *et al.* (37) realized that particles

must grow to millimeter sizes to reduce several percent supersaturation to saturation conditions.
 26. R. M. Goody, Y. L. Yung, *Atmospheric Radiation, Theoretical Basis* (Oxford Univ. Press, Oxford, 1989).
 27. R. Courtin *et al.*, *Icarus* **114**, 144 (1995).
 28. R. E. Samuelson *et al.*, *Planet. Space Sci.* **45**, 959 (1997).
 29. H. Stommel, *J. Meteorol.* **4**, 91 (1947).
 30. J. Simpson, G. W. Brier, R. H. Simpson, *J. Atmos. Sci.* **24**, 508 (1967).
 31. O. B. Toon, C. P. McKay, R. Courtin, T. P. Ackerman, *Icarus* **75**, 255 (1988).
 32. P. Gierasch, R. Goody, P. Stone, *Geophys. Fluid Dyn.* **1**, 1 (1970)
 33. C.A.G. and J.L.H. are supported by the NASA Planetary Astronomy Program under grant NAG5-6790.

18 July 2000; accepted 21 September 2000

Acute Sensitivity of Landslide Rates to Initial Soil Porosity

R. M. Iverson,¹ M. E. Reid,² N. R. Iverson,³ R. G. LaHusen,¹ M. Logan,¹ J. E. Mann,³ D. L. Brien²

Some landslides move imperceptibly downslope, whereas others accelerate catastrophically. Experimental landslides triggered by rising pore water pressure moved at sharply contrasting rates due to small differences in initial porosity. Wet sandy soil with porosity of about 0.5 contracted during slope failure, partially liquefied, and accelerated within 1 second to speeds over 1 meter per second. The same soil with porosity of about 0.4 dilated during failure and slipped episodically at rates averaging 0.002 meter per second. Repeated slip episodes were induced by gradually rising pore water pressure and were arrested by pore dilation and attendant pore pressure decline.

In popular metaphor, landslide processes begin spontaneously and gain momentum as they proceed, but what determines how real landslides move? Can small differences in initial conditions cause some landslides to accelerate catastrophically and others to creep intermittently downslope? The distinction is important because rapid landslides pose lethal threats, whereas slow landslides damage property but seldom cause fatalities (1).

A longstanding hypothesis holds that landslide behavior may depend on initial soil porosity, because soils approach specific critical-state porosities during shear deformation (2–4). Tests on small soil specimens indicate that dense soils (initially less porous than critical) dilate as they begin to shear, whereas loose soils (initially more porous than critical) contract (5–7). Dilation can reduce pore water pressures and thereby retard continued deformation by increasing normal stresses and frictional strength at grain contacts, whereas contraction can increase pore water pressures and thereby reduce frictional

strength (8–10). Positive feedback between frictional strength reduction and soil contraction may cause some landslides to transform into liquefied high-speed flows (11–13).

To isolate the effect of initial soil porosity on landslide style and rate, we conducted large-scale experiments under closely controlled conditions. In each of nine landslide experiments, we placed a 65-cm-thick, 6-m³ rectangular prism of loamy sand soil (Table 1) on a planar concrete bed inclined 31° from horizontal and bounded laterally by vertical concrete walls 2 m apart (Fig. 1). The downslope end of each soil prism was restrained by a rigid wall, which ensured that deformation occurred at least partly within the soil mass (rather than along the bed) and that landsliding included a rotational component.

Different methods of soil placement yielded different initial porosities. The highest porosities (>0.5) were attained by dumping the soil in 0.5-m³ loads and raking it into position, without otherwise touching its surface. Lower porosities resulted from placing the soil in 10-cm layers parallel to the bed and compacting each layer with either foot traffic or 16-Hz mechanical vibrations that delivered impulsive loads of ~2 kPa at depths of 10 cm (14). After placement of each soil prism, we determined porosities by excavating four to nine ~1-kg samples at

various depths and measuring their volumes, masses, and water contents (15). No systematic variations of porosity with depth were detected.

Our suite of landslide experiments included individual tests with initial porosities ranging from 0.39 ± 0.03 to 0.55 ± 0.01 (± 1 SD sampling error for an individual experiment). Ancillary tests of the same soil in a ring-shear device and triaxial cell produced dilative shear failure when initial porosity was ≤ 0.41 and contractive shear failure when initial porosity was ≥ 0.46 (Fig. 2 and Table 1). Landslides with initial porosities that bracketed the range from 0.41 to 0.46 were therefore of greatest interest.

Landslide motion was measured with two ground-surface extensometers and 17 or 18 subsurface tiltmeters arranged at depth increments of ~7 cm in two vertical nests (16). Pore water pressures were measured with 12 tensiometers and 12 dynamic piezometers arranged in three vertical nests at depth increments of ~20 cm (17) (Fig. 1). Data from each sensor were logged digitally at 20 Hz for the duration of each experiment.

To induce landsliding, soil prisms were watered with surface sprinklers and through subsurface channels that introduced simulated groundwater (Fig. 1). Rising water tables were kept nearly parallel to the impermeable bed by adjusting discharge from a drain at the base of the retaining wall. Although preliminary experiments indicated that different styles and rates of water application influenced the onset of slope failure, this influence became negligible as failure occurred and instigated changes in soil porosity (18, 19).

Landslides with differing porosities displayed sharply contrasting dynamics (compare Figs. 3 and 4). Each of four landslides with initial porosities >0.5 failed abruptly and accelerated within 1 s to speeds >1 m/s. The surfaces of these landslides appeared fluid and smooth, and data from dynamic piezometers confirmed that pore water pressures rose rapidly during failure and reached levels nearly sufficient to balance total normal stresses and liquefy the soil (Fig. 3). Three landslides with

¹U.S. Geological Survey, 5400 MacArthur Boulevard, Vancouver, WA 98661, USA. ²U.S. Geological Survey, 345 Middlefield Road, Menlo Park, CA 94025, USA. ³Department of Geological and Atmospheric Sciences, Iowa State University, Ames, IA 50011, USA.